

Solving eigenvalue problems obtained by the finite element method on a quantum annealer using only a few qubits

Arnaud Rémi¹, François Damanet², and Christophe Geuzaine¹

¹Department of Electrical Engineering and Computer Science, Institut Montefiore, University of Liège, 4000 Liège, Belgium

²Institut de Physique Nucléaire, Atomique et de Spectroscopie, CESAM, University of Liège, 4000 Liège, Belgium

October 18, 2024

Abstract

One of the main obstacles for achieving a practical quantum advantage in quantum computing lies in the relatively small number of qubits currently available in quantum hardware. Here, we show how to circumvent this problem in the context of eigenvalue problems obtained by the finite element method, via the use of an adaptive algorithm for quantum annealers – the Adaptive Quantum Annealer Eigensolver (AQAE) – in a way that only a few qubits are required to achieve a high precision. As an example, we apply AQAE to eigenvalue problems that are relevant in a wide range of contexts, such as electromagnetism, acoustics and seismology, and quantify its robustness against different types of experimental errors. Our approach could be applied to other algorithms, and makes it possible to take the most of current Noisy-Intermediate-Scale Quantum devices.

1 Introduction

Over the last decades, quantum computing has emerged as a crucial field to invest in [1], given its potential to solve computational problems that are intractable for classical computers [2, 3, 4]. On the hardware side, two classes of platforms hold their own: i) universal gate-based quantum computers, which make it possible to perform arbitrary calculations, and ii) quantum annealers [5], which allow for solving specific optimization problems that can be mapped into Ising [or equivalently quadratic unconstrained binary optimization (QUBO)] problems. While quantum annealers seem more restrictive than gate-based quantum computers, they are in fact equivalent [6], although depending on the problem to solve one approach is usually more natural than the other. In this context, as Ising problems belong to the NP-hard computational complexity class [7], quantum annealers are well-suited for solving a wide range of real-life problems, ranging from protein folding with health applications to finance, linear algebra or logistics.

However, despite the fast development of quantum hardware, the current numbers of qubits available as well as their fragility against noise have hindered, up to now, the achievement of practical quantum advantages [8, 9]. Yet, anticipating the advent of large-scale fault-tolerant quantum computers, many quantum algorithms with applications in various fields [10] have been developed. Here, we investigate how to take the most of the existing Noisy-Intermediate-Scale Quantum (NISQ) devices by reducing the amounts of qubits required to perform a desired calculation. In this paper, we use an iterative algorithm, the Adaptive Quantum Annealing Eigensolver (AQAE) [11], based on the Quantum Annealing Eigensolver (QAE) presented in [12], that makes it possible to solve eigenvalue problems with high precision using only a few qubits. This approach has been used for solving eigenvalue problems, e.g., in the contexts of molecular physics [11, 13] or the computation of relativistic excitation energies [14], but, to the best of our knowledge, never in the context of finite element methods. Here, we use the AQAE for computing the eigenvalues and eigenvectors of the discretized Laplacian operator, and study the impact of experimental errors that can occur in the hardware on the robustness of the algorithm.

Our paper is organized as follow. In Section II, we present background on quantum annealing and on the variational formulation of eigenvalue problems. In Section III, we summarize the Quantum Annealing Eigensolver (QAE) of Ref. [12] and detail our implementation of its adaptative generalization (AQAE) initially developed in Ref. [11]. In Section IV, we benchmark our algorithm to the finding of the eigenvalues and eigenvectors of the Laplacian operator discretized via the finite element method. There, we compare the performances of AQAE when the quantum annealing part is performed on a real quantum annealer provided by Dwave with direct calculations of the QUBO solution as if the annealing was ideal (adiabatic computation). Finally, in Section V, we conclude and present a few perspectives of our work.

2 Background

In this section, we first review the basics of quantum annealing, highlighting the main sources of errors of the method. Then, as quantum annealers can only solve optimization problems, we present the variational formulation of generalized eigenvalue problems (gEVPs) involving hermitian operators based on the min-max theorem.

2.1 Quantum annealing

Quantum annealing (QA) is a metaheuristics, i.e, a method to find (sufficiently good) solutions of optimization problems, performed by quantum annealers. To do so, the qubits in the hardware are first initialised in a easy-to-prepare ground state of a Hamiltonian H_0 . Then, their interactions are adiabatically adapted until reaching the values of the parameters J_{kl} and h_k of a classical Ising Hamiltonian H_p encoding the solution of the optimization problem of interest and of the form

$$H_p = \sum_{\alpha} h_{\alpha} s_{\alpha} + \sum_{\alpha, \beta} J_{\alpha\beta} s_{\alpha} s_{\beta}, \quad (1)$$

where $s_{\alpha} = \{-1, 1\}$ are the spin variables stored in the qubits states. The time-dependent Hamiltonian governing the quantum annealing dynamics can be parametrized as follows

$$H(s) = A(s)H_0 + B(s)H_p, \quad s \in [0, 1], \quad (2)$$

where $s = t/t_a$ is an adimensional parameter with t_a the total annealing time, and A and B time-dependent scheduling parameters with typically $A(0) \gg B(0)$ and $A(1) \ll B(1)$ so that $H(0) \propto H_0$ and $H(1) \propto H_p$. According to the adiabatic quantum theorem, if the Hamiltonian $H(s)$ evolves sufficiently slowly, the quantum state of the system should remain in the instantaneous ground state of $H(s)$ for all times, thereby evolving towards the ground state of H_p for $s = 1$ [15, 16], i.e., to the spin configuration optimizing the problem, which can be extracted via direct measurement of the qubits at the end of the quantum annealing process. The minimum energy gap between the ground state and the first excited state is denoted by Δ , and represents a key parameter to determine the annealing time t_a , as typically one requires $t_a \gg 1/\Delta^2$ [15, 17], although other studies suggested $t_a \gg \Delta^{-3}$ [18] or $t_a \gg \Delta^{-2} |\log \Delta|^\beta$ [19], which ultimately depends on the specific form of $H(s)$. Nevertheless, the choice of the annealing time represents a possible source of errors. Another source is the decoherence induced by the coupling of the hardware to its environment, which actually suggests the existence of a tradeoff for choosing t_a as larger t_a implies stronger decoherence effects. Finally, other errors can come from a bad encoding of the values of J_{kl} and h_k in the hardware, as deviations from the right values might modify the ground state, or more generally from the approximations used to obtain the Ising Hamiltonian or from the binarization procedure of the variables when one has to deal with real values problems, as elaborated below in our examples.

Finding the ground state of an Ising Hamiltonian of the form (1) is strictly equivalent to finding the solution of a Quadratic Unconstrained Binary Optimization (QUBO) problem of the form

$$\mathbf{q}_\star = \arg \min_{\mathbf{q}} \mathbf{q}^T Q \mathbf{q}, \quad \mathbf{q} \in \{0, 1\}^D, \quad (3)$$

where the binary variables q_α that are the components of the vector \mathbf{q} of dimension D are simply related to the spin variables through $q_\alpha = (s_\alpha + 1)/2$, and where the \star symbol denotes the optimized value of \mathbf{q} . Higher order binary polynomial functions can be minimized using QA by expressing as binary quadratic function at the price of additional binary variables [20, 21]. In the following, we will be interested in formulating the solution of an eigenvalue problem as a QUBO of the form (3), keeping in mind that it is equivalent to the Ising model (1) natively implemented in the hardware.

2.2 Variational formulation of eigenvalue problems

Let us consider the following generalized Eigenvalue Problem (gEVP)

$$H\phi = \lambda M\phi, \quad (4)$$

where H is a hermitian operator of dimension $N \times N$, M positive definite, and λ and \mathbf{u} the eigenvalues and eigenvectors of the gEVP, respectively. The solution of such problems are pairs of eigenvalues and eigenvectors labelled as $\{\lambda_k, \phi_k\} = \{\lambda, \phi\}$ ($k = 0, \dots, N - 1$). The min-max theorem allows to formulate the search of eigenpairs of an eigenvalue problem (standard or generalized) as a variational problem of the form (see App. A.1)

$$\lambda_k = \min_{\phi \in \mathcal{S}_k} \frac{\phi^\dagger H \phi}{\phi^\dagger M \phi}, \quad (5)$$

$$\phi_k = \arg \min_{\phi \in \mathcal{S}_k} \frac{\phi^\dagger H \phi}{\phi^\dagger M \phi}, \quad (6)$$

with \cdot^\dagger the conjugate transpose operator, and $\mathcal{S}_k = \text{span}(\phi_k, \dots, \phi_{N-1})$. It can be shown that solving Eqs.(5)-(6) is equivalent to solving

$$\lambda_k = \min_{\phi \in \mathcal{S}_k} \phi^\dagger H \phi \quad : \quad \phi^\dagger M \phi = 1, \quad (7)$$

$$\phi_k = \arg \min_{\phi \in \mathcal{S}_k} \phi^\dagger H \phi \quad : \quad \phi^\dagger M \phi = 1. \quad (8)$$

or

$$\lambda_k = \min_{\gamma \in \mathbb{R}, \phi \in \mathcal{S}_k} \phi^\dagger H \phi - \gamma(\phi^\dagger M \phi - 1), \quad (9)$$

$$\phi_k = \arg \min_{\gamma \in \mathbb{R}, \phi \in \mathcal{S}_k} \phi^\dagger H \phi - \gamma(\phi^\dagger M \phi - 1), \quad (10)$$

using Lagrange multiplier method where γ is the Lagrange multiplier. This formulation allows to compute all the eigenvalue-eigenvector pairs iteratively starting with $k = 0$ and $\mathcal{S}_0 = \mathbb{C}^N$.

3 Algorithms

In this section, we first review and slightly generalize the quantum annealer eigensolver (QAE) designed in Ref. [12] to deal with gEVP. Then, we detail our implementation of the Adaptive Quantum Annealer Eigensolver (AQAE) [11], allowing for using fewer qubits while keeping a high precision.

3.1 Quantum annealer eigensolver

The idea of using the min-max theorem to solve standard eigenvalue problems on a quantum annealer comes, at first, from Ref. [12] and has various follow-ups [22, 23, 24, 25]. This section is aimed to introduce the quantum annealer eigensolver (QAE) [12] generalized to gEVPs. This solver does only handle quadratic unconstrained binary optimization problems (QUBOs), hence a mapping between gEVPs and QUBOs has to be established.

3.1.1 Towards a quadratic problem

The optimization problems in Eqs. (9)-(10) are quadratic in ϕ , but globally non quadratic since γ is a variable of the problem. The idea used in Ref. [12] comes from the observation that if $\gamma < \gamma_*$, the trivial solution $\phi_* = \mathbf{0}$ is favorised while it is not when $\gamma > \gamma_*$. Using this observation, γ can be seen as a fixed parameter that is iteratively updated until it converges towards γ_* . Alg. 1 can, e.g., be used to reach γ_* . The initial bounds γ_{\min} and γ_{\max} are chosen such that $\gamma = \gamma_{\min}$ leads to the trivial solution while $\gamma = \gamma_{\max}$ does not.

3.1.2 Binarization

In Ref. [12], each continuous variable ϕ_j ($j = 0, \dots, N - 1$), i.e., each component of ϕ , is mapped to binary string \mathbf{q}_j as follows

$$\phi_j(\mathbf{q}_j) = \sum_{k=1}^{K-1} 2^{k-K} q_{jk} - q_{jK} \in [-1, 1),$$

Algorithm 1 Algorithm for γ_* -search in QAE

Require: $H, M, \gamma_{\min}, \gamma_{\max}, N_\gamma$
Ensure: $\gamma = \gamma_*$

```

1:  $\gamma \leftarrow (\gamma_{\min} + \gamma_{\max})/2$ 
2:  $i \leftarrow 0$ 
3: while  $i < N_\gamma$  do
4:    $\phi_*(\gamma) \leftarrow \arg \min_{\phi} \phi^\dagger H \phi - \gamma \phi^\dagger M \phi$ 
5:   if  $\phi_*(\gamma) = \mathbf{0}$  then
6:      $\gamma_{\min} \leftarrow \gamma$ 
7:   else
8:      $\gamma_{\max} \leftarrow \gamma$ 
9:   end if
10:   $i \leftarrow i + 1$ 
11: end while
12: return  $\gamma_{\max}$ 

```

where K is the number of binary variables that expand ϕ_j , which we take independent of j for simplicity. By applying this transformation, the optimization problem given by Eqs. (9)-(10) has a QUBO formulation

$$\mathbf{q}_* = \arg \min_{\mathbf{q}} \mathbf{q}^T (Q_H - \gamma Q_M) \mathbf{q}, \quad (11)$$

with $\mathbf{q} \in \{0, 1\}^{NK}$ and $Q_H, Q_M \in \mathbb{R}^{NK \times NK}$. The construction of Q_H and Q_M is detailed in App. A.2.

3.1.3 Towards an unconstrained problem

The optimization problem shown in Eq. (11) is constrained by the space spanned by $\phi(\mathbf{q})$. In order to make it unconstrained, the restriction $\phi \in \mathcal{S}_k$ can be made by adding a penalization term ξ_k for vectors that are not M -orthogonal to span $(\phi_0, \dots, \phi_{k-1})$, of the form

$$\xi_k(\phi) = \sum_{m=0}^{k-1} \beta_m (\phi^\dagger M \phi_m)^2 = \sum_{m=0}^{k-1} \beta_m \phi^\dagger P_{M, \phi_m} \phi, \quad (12)$$

where $P_{M, \phi_m} = M \phi_m \phi_m^\dagger M^\dagger$ and $\beta_m > \lambda_k - \lambda_m$ [12, 26]. In terms of the binary variables \mathbf{q} , this leads to

$$\xi_k(\mathbf{q}) = \sum_{m=0}^{k-1} \beta_m (\phi_{\min}^T P_{M, \phi_m} \phi_{\min} + \mathbf{q}^T Q_{P_{M, \phi_m}} \mathbf{q}), \quad (13)$$

where $Q_{P_{M, \phi_m}}$ is derived from the binarization of ϕ . This penalization being introduced in Syst. (11), the optimization problem becomes

$$\boxed{\begin{cases} \mathbf{q}_* &= \arg \min_{\mathbf{q}} \mathbf{q}^T Q \mathbf{q} + \xi_k(\mathbf{q}), \\ \phi_k &= \phi(\mathbf{q}_*), \\ \lambda_k &= \phi_k^\dagger H \phi_k / \phi_k^\dagger M \phi_k. \end{cases}} \quad (14)$$

The optimization problem described in Syst. (14) is the QUBO formulation of the generalized eigenvalue problem. The QAE described in [12] consists in iteratively solving these QUBOs until a γ_* is reached with enough precision. The whole QAE algorithm is schematized in Fig. 1.

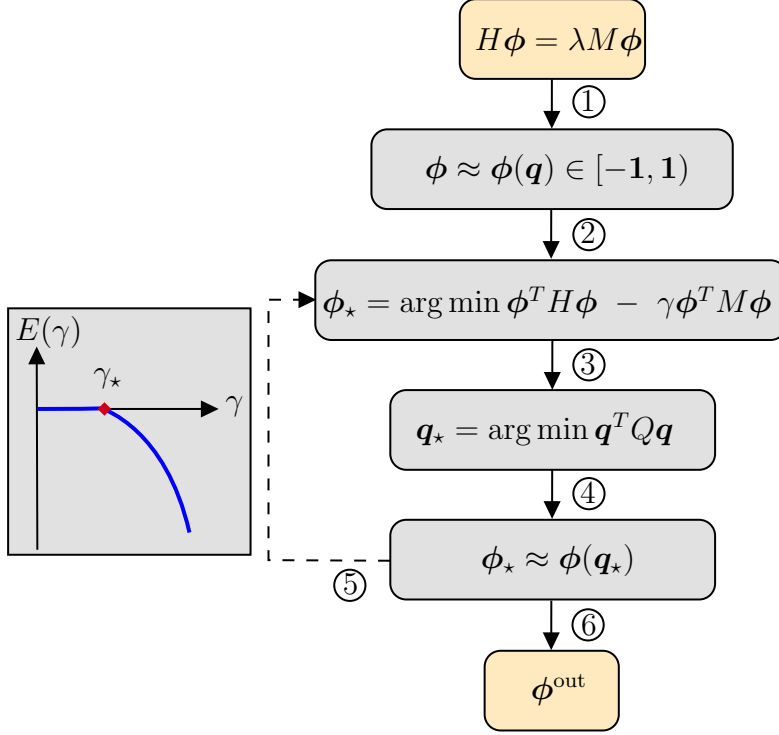


Figure 1: Quantum annealer eigensolver algorithm. (1) Binarization of the continuous variables; (2) Continuous variational formulations; (3) QUBO formulation solved with quantum annealing; (4) Reconstruct continuous variables based on binary solution; (5) If γ_* is not reached, update γ and go back to step 2. The graph on the left shows the typical shape of $E(\gamma)$ and γ_* ; (6) Output current solution.

3.2 Adaptive Quantum Annealer Eigensolver

Current limitations in quantum hardware limit the size of the problems that can be solved using quantum annealers. As of 2024, the quantum annealer of D-Wave counts 5000 qubits. However, the connectivity between these qubits being limited, only very sparse problems can be solved using 5000 qubits simultaneously. For dense problems, the maximum number of qubits is currently around 100, which is significantly less [27].

A problem with N real variables each discretized with K binary variables requires $N \times K$ qubits to be solved on a quantum annealer. This means that QAE can currently only solve small problems with a coarse precision. The aim of the adaptive quantum annealer eigensolver (AQAE) is to solve problems with arbitrarily high precision despite the restricted number of qubits. The error $\epsilon_{j,K}$ of the discretization on the component ϕ_j is defined as follows

$$\epsilon_{j,K} \sim 2^{-K} \delta, \quad \delta = (\phi_{j,\max} - \phi_{j,\min}).$$

The core idea of AQAE [11] is to solve at the current precision, and to iteratively use the box algorithm [28] to iteratively refine δ around the current coarse solution to reduce the discretization error at fixed K until the target precision is reached. The box algorithm combined with QA has recently been used for solving other engineering problems [28, 29, 30] using quantum hardware. AQAE differs from QAE in two points. The first is the routine for the γ_* -search. As the algorithm refines the bounds within which the continuous variables are defined, the trivial solution $\phi_* = \mathbf{0}$ is not necessarily feasible. Therefore, the criterion for the γ -bounds update has to be revisited.

Algorithm 2 is based on the observation that the function $\phi^\dagger H \phi - \gamma \phi^\dagger M \phi$ is strictly positive if and only if $\gamma < \gamma_*$. Hence, its minimum value can be used as a criterion to update γ .

Algorithm 2 Algorithm for γ_* -search in AQAE

Require: $H, M, \gamma_{\min}, \gamma_{\max}, N_\gamma$

Ensure: $\gamma = \gamma_*$

```

1:  $\gamma \leftarrow (\gamma_{\min} + \gamma_{\max})/2$ 
2:  $i \leftarrow 0$ 
3: while  $i < N_\gamma$  do
4:    $E(\gamma) \leftarrow \min_\phi \phi^\dagger H \phi - \gamma \phi^\dagger M \phi$ 
5:   if  $E(\gamma) \geq 0$  then
6:      $\gamma_{\min} \leftarrow \gamma$ 
7:   else
8:      $\gamma_{\max} \leftarrow \gamma$ 
9:   end if
10:   $i \leftarrow i + 1$ 
11: end while
12: return  $\gamma_{\max}$ 

```

The next major difference between QAE and AQAE is the δ -refinement steps. This refinement requires the bounds ϕ_{\min}, ϕ_{\max} to appear explicitly in the binarization at each iteration m of the box algorithm. Hence, in IQAE the mapping between a continuous ϕ_j and a binary string \mathbf{q}_j is the following

$$\phi_j \approx \phi_{j,\min}^{(m)} + \mathbf{b}^T \mathbf{q}_j, \quad \text{with} \quad b_k = (\phi_{j,\max}^{(m)} - \phi_{j,\min}^{(m)}) \times 2^{-k}, \quad (k = 0, \dots, K-1), \quad (15)$$

which, as in QAE, leads to a QUBO of the form

$$\begin{cases} \mathbf{q}_* &= \arg \min_{\mathbf{q}} \mathbf{q}^T Q \mathbf{q}, \\ \phi_k &= \phi(\mathbf{q}_*), \\ \lambda_k &= \phi_k^\dagger H \phi_k / \phi_k^\dagger M \phi_k. \end{cases}$$

The mathematical construction of Q and $\xi_k(\mathbf{q})$ is detailed in Appendix A. The box algorithm for the δ -refinement is detailed in Alg. 3. Finally, the complete AQAE algorithm is sketched in Fig. 2. The binarization (15) is asymmetric with respect to the current solution. In our work, we chose to symmetrize the binarization by adding a shift to the $\phi_{j,\min}$ which appears to lead to better convergence of the algorithm in the cases investigated. The details about the AQAE algorithm scaling can be found in Ref. [11].

Algorithm 3 Box algorithm in AQAE

Require: $H, M, \alpha, \epsilon_*, \delta_0, N_\delta$

- 1: $\delta \leftarrow \delta_0$
 - 2: $\epsilon \leftarrow 2^{-K}\delta$
 - 3: $m \leftarrow 0$
 - 4: **while** $m < N_\delta$ **do**
 - 5: **compute** γ_* using Alg. 2
 - 6: $\phi_* \leftarrow \arg \min_{\phi} \phi^\dagger H \phi - \gamma_* \phi^\dagger M \phi$
 - 7: $\delta \leftarrow \alpha \delta$
 - 8: $\epsilon \leftarrow 2^{-K} \delta$
 - 9: $\phi_{\min} \leftarrow \phi_* - \delta/2$
 - 10: $\phi_{\max} \leftarrow \phi_* + \delta/2$
 - 11: $m \leftarrow m + 1$
 - 12: **end while**
-

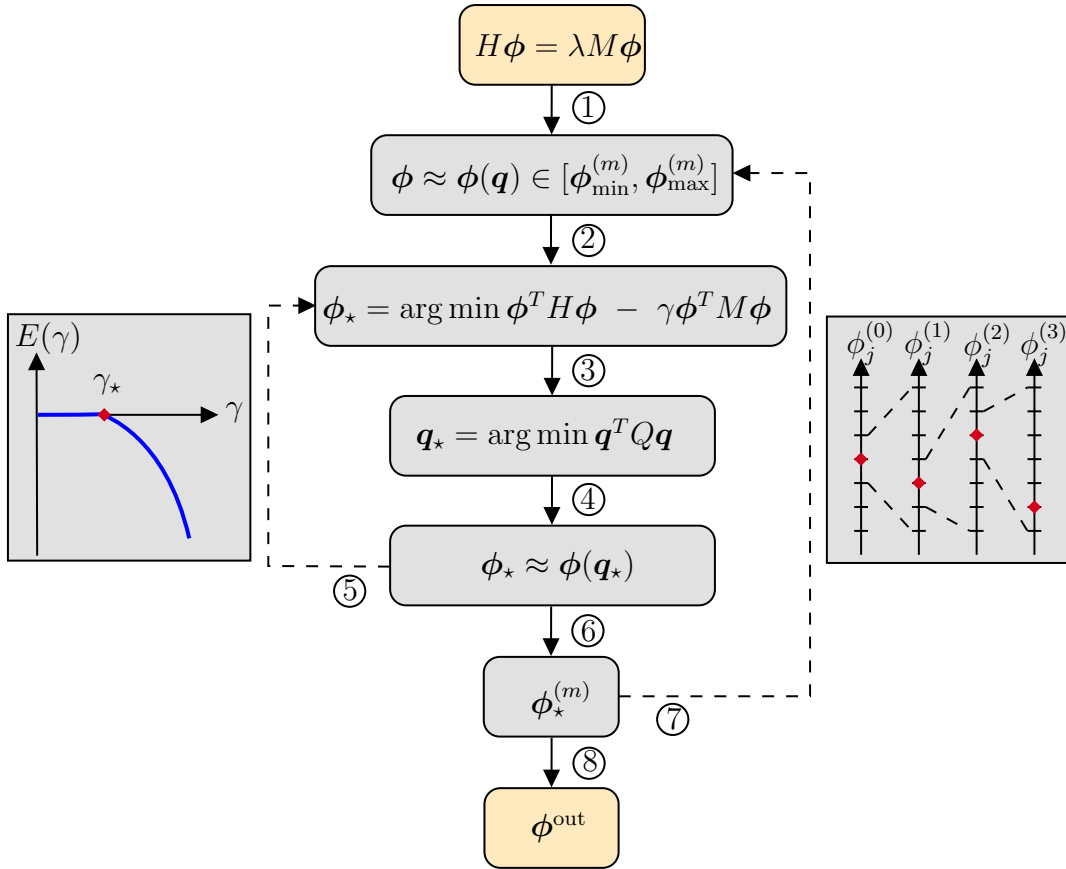


Figure 2: Adaptive quantum annealer eigensolver algorithm. (1) Binarization of the continuous variables; (2) Continuous variational formulations; (3) QUBO formulation solved with quantum annealing; (4) Reconstruct continuous variables based on binary solution; (5) If γ_* is not reached, update γ using Alg. 2 and go back to step 2. The graph on the left shows the typical shape of $E(\gamma)$ and γ_* ; (6) Outputs current solution; (7) If target precision is not reached, update δ using Alg. 3 and go back to step 1. The graph on the right shows the effect of the box algorithm on the bounds; (8) Output final solution

4 Applications

In this section, AQAE will be used to solve a specific gEVP arising from the discretization of the wave equation in the frequency domain. In the current study, only the one-dimensional problem will be solved in a medium that contains two materials with different electromagnetic properties. The solutions of this problem are the eigenmodes and their corresponding frequencies. At first, the gEVP will be derived from the boundary value problem. Afterwards, the problem will be solved using AQAE, starting with a small-scale problem ($NK = 6$) run on real hardware in order to benchmark the method against other approaches, before investigating a larger problem ($NK = 50$). Throughout the section, we also address the impact of experimental errors on the success of the method.

4.1 The eigenvalue problem

The one-dimensional boundary value problem that we consider is

$$\begin{cases} \frac{1}{\varepsilon\mu} \frac{\partial^2 \phi(x, \omega)}{\partial x^2} = -\omega^2 \phi(x, \omega), & x \in [0, L], \\ \{\varepsilon, \mu\} = \{\varepsilon_1, \mu_1\}, & x \in [0, l], \\ \{\varepsilon, \mu\} = \{\varepsilon_2, \mu_2\}, & x \in]l, L], \\ \phi|_{x=0} = \phi|_{x=L} = 0, \end{cases} \quad (16)$$

where ε and μ are the electric and the magnetic permittivity respectively; L is the total length of the medium, and $l < L$ is the length spanned by the first dielectric material. The problem described by Eq. (16) is a continuous eigenvalue problem for the operator $1/\varepsilon\mu \times \partial^2/\partial x^2$. A discrete eigenvalue problem can be obtained by using the finite element method to discretize Eq. (16). First of all, let us introduce the weak formulation of this system by multiplying it with a test function v and integrating by parts

$$\int_{\Omega} \frac{1}{\varepsilon\mu} \frac{\partial \phi}{\partial x} \frac{\partial v}{\partial x} dx = \omega^2 \int_{\Omega} \phi v dx.$$

Note that $v(0) = v(L) = 0$ has been assumed, as there are no Neumann boundary conditions for ϕ . A discrete version of the weak formulation can be obtained by approximating ϕ by N shape functions $\varphi_1, \dots, \varphi_N$ defined on compact supports as

$$\phi(x) \approx \sum_{j=1}^N \phi_j \varphi_j(x), \quad (17)$$

with coefficients ϕ_j . The weak formulation becomes

$$\sum_{j=1}^N \underbrace{\int_{\Omega} \frac{1}{\varepsilon\mu} \frac{\partial \varphi_i}{\partial x} \frac{\partial \varphi_j}{\partial x} dx}_{H_{ij}} \phi_j = \omega^2 \sum_{j=1}^N \underbrace{\int_{\Omega} -\varphi_i \varphi_j dx}_{M_{ij}} \phi_j,$$

where H is the discretized Laplacian operator divided by the square wave velocity, and M represents the inner product of the shape functions. Since eigenvalue shifts do not disturb eigenvectors of operators, solutions ϕ_j can be found by solving

$$H\phi = \omega^2 M\phi, \quad (18)$$

that is, a generalized eigenvalue problem for the pair (H, M) . Such generalized eigenvalue problems can be converted into standard eigenvalue problems at the cost of computing M^{-1} . Note that if the shape functions are chosen to be mutually orthogonal (i.e., $(\varphi_i, \varphi_j) = \delta_{ij}$), M is diagonal, and we directly recover a standard eigenvalue problem. In its variational form, the gEVP becomes

$$\begin{cases} \lambda_k = \min_{\phi \in \mathcal{S}_N} \frac{\phi^\dagger H \phi}{\phi^\dagger M \phi} \approx \min_{\mathbf{q}} \mathbf{q}^T Q_H \mathbf{q} - \gamma \mathbf{q}^T Q_M \mathbf{q} + \sum_{m=0}^{k-1} \beta_m \mathbf{q}^T Q_{P_{\phi_m}} \mathbf{q}, \\ \phi_k = \arg \min_{\phi \in \mathcal{S}_N} \frac{\phi^\dagger H \phi}{\phi^\dagger M \phi} \approx \arg \min_{\mathbf{q}} \mathbf{q}^T Q_H \mathbf{q} - \gamma \mathbf{q}^T Q_M \mathbf{q} + \sum_{m=0}^{k-1} \beta_m \mathbf{q}^T Q_{P_{\phi_m}} \mathbf{q}. \end{cases} \quad (19)$$

4.2 Results

In the following subsection, the problem above will be solved in \mathbb{R}^3 and \mathbb{R}^{25} using 6 and 50 qubits respectively, i.e., with only $K = 2$ qubits per continuous variable.

4.2.1 Generalized eigenvalue problem with 6 qubits

The 6-qubit problem consists in i) writing the gEVP of Eq. (18) with $\phi(\mathbf{q}) \in \mathbb{R}^N$ with $N = 3$, that is, using $N = 3$ shape functions $\varphi_j(x)$ in Eq. (17), and ii) discretizing each continuous variable ϕ_j using $K = 2$ binary variables. In total, this leads to $N \times K = 6$ binary variables, that is, $\mathbf{q} \in \{0, 1\}^6$. The medium is considered as a homogeneous vacuum ($\varepsilon_1 = \varepsilon_2 = \varepsilon_0$, $\mu_1 = \mu_2 = \mu_0$).

The solution for the 6-qubit Helmholtz problem using AQAE (solver parameters listed in App. B) is shown in Fig. 3 for the first eigenmode together with relative errors on ϕ and λ , respectively, as well as the relative residual defined as $|H\phi - \lambda M\phi|^{(m=N_\delta-1)} / |H\phi - \lambda M\phi|^{(m=0)}$. Different t_a , QUBO solver types (D-Wave’s quantum annealer (QA) and simulated annealing solver (SA) [31]) and number of samples per QUBOs are considered and compared with the ideal (adiabatic) results of the algorithm. At first, we notice that the annealing does not necessarily need to be perfectly adiabatic for the method to work, as the adiabatic solution is not the only one to converge. Furthermore, it happens that AQAE with heuristic QUBO solvers (QA and SA) outperforms the adiabatic results in terms of errors and residual at some points. The iterative algorithm success should however be related to how close its solution evolution is to the one that is theoretically expected (i.e., if the adiabatic theorem holds, for infinite annealing time). We therefore notice that the success of AQAE is sensitive to the number of samples per QUBO, which has been observed in other quantum annealing-assisted algorithms (e.g., Ref. [30]). For problems of this size, increasing t_a from 1 μs to 10 μs did not improve the results significantly.

4.2.2 Generalized eigenvalue problem with 50 qubits

The fact that arbitrarily high precision can be reached with only 2 binary variables per continuous variable using AQAE allows us to handle larger problems than the ones that have previously solved in [12, 22, 23]. This section is aimed at solving Eq. (18) in \mathbb{R}^{25} with high precision using only 50 qubits using AQAE. The problem has been solved in two different cases: i) in homogeneous vacuum ($\varepsilon_1 = \varepsilon_2 = \varepsilon_0$, $\mu_1 = \mu_2 = \mu_0$) ii) in heterogeneous SiO₂-vacuum ($\varepsilon_1 = 3.9 \times \varepsilon_0$, $\varepsilon_2 = \varepsilon_0$, $\mu_1 = \mu_2 = \mu_0$, $l = L/2$). The AQAE is performed with parameters detailed in App.B. Fig. 4 shows the output solution of AQAE as well as the evolution of the errors in terms of ϕ , λ and the relative residual of the gEVP with the box algorithm iterations for the first three eigenmodes of Eq. (18). As observed in Fig. 4(a), the AQAE was able to converge towards the solution in vacuum using

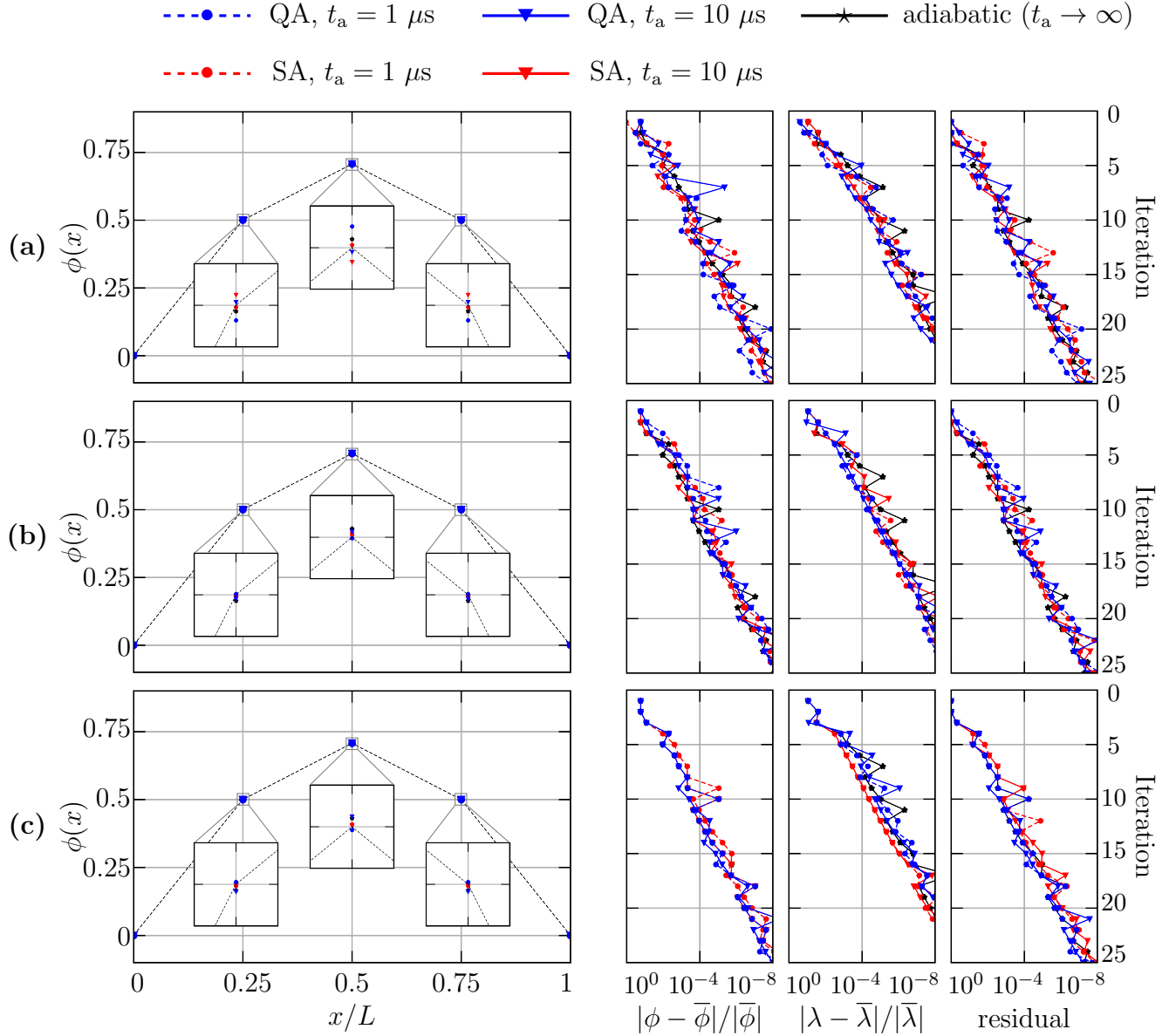


Figure 3: **6-qubit gEVP problem:** solution of the gEVP using the AQAE algorithm ($\phi(x)$ in colored markers) and a classical gEVP solver ($\bar{\phi}(x)$ in dashed lines) in a homogeneous material (vacuum) using D-Wave’s quantum annealer (QA in blue) and classical simulated annealing algorithm (SA in red) with various annealing times and drawing 1 (a), 4 (b) or 8 (c) samples per QUBO. The boxes that zoom on ϕ are $\Delta_0 \times \alpha^{N_\delta} \approx 6 \times 10^{-8}$ side. For simulated annealing, the annealing time is defined as $t_a = N_{\text{flips}}\tau$ where N_{flips} is the total number of spin-flips occurring during the annealing process and $\tau = 10$ ns a characteristic time chosen arbitrarily for spin flips.

real quantum hardware. It is not the case for the heterogeneous SiO₂-vacuum material, as observed in Fig. 4(b). It does however converge if AQAE is performed on classical hardware as shown in Fig. 4(c). As mentioned earlier, there are three major kinds of error sources in D-Wave’s quantum annealers : i) errors due to the fact that the process is non-adiabatic in practice, the annealing time being finite and often too small, ii) errors due to noise in the quantum processor [32, 33], iii) integrated control errors (ICE) [27], i.e., errors in the mapping between the QUBO and the qubits interactions in the quantum annealer. We believe that ICE are the major cause of the algorithm failing, and that the fact that ICE lead to convergence issues or not is problem dependent. In order to evaluate how ICE can lead to convergence issues, we model ICE by an additional gaussian contribution in the QUBOs

$$Q_{\text{eff}} = Q + \delta Q, \quad \delta Q_{ij} = \eta_{ij} |Q_{\text{max}}|,$$

where $\eta_{ij} \sim \mathcal{N}(0, \sigma_\eta)$ and $|Q_{\text{max}}|$ is the maximum value of Q in absolute terms. Fig. 5 shows the amount of orders of magnitudes that separate the error at the first and last AQAE iteration for the computation of the first eigenmode, with respect to σ_η which quantifies the ICE magnitude. Let us define the critical ICE magnitude σ_η^* as the ICE above which the AQAE does not converge. For the homogeneous vacuum case we find $\sigma_\eta^*/|Q_{\text{max}}| \approx 0.006$ (see Fig. 5(A)), while for the SiO₂-vacuum case we find $\sigma_\eta^*/|Q_{\text{max}}| \approx 0.002$ (see Fig. 5(B)). This confirms that the critical ICE is problem dependent. The critical ICE can be seen as the problem representation error that changes the optimal spin configuration, which depends on the energy spectrum which is problem dependent. In D-Wave’s quantum annealer, ICE magnitude are of this same order of magnitude [27] and can therefore cause modifications in the eigenstates of some problems, as it is the case for the Helmholtz problem with heterogeneous SiO₂-vacuum material here. Figs. 6 and 7 show the shape of the eigenmodes found using AQAE for a wide range of ICE magnitudes.

Conclusion

The adaptive quantum annealing eigensolver (AQAE) has been used to solve eigenvalue problems obtained by the finite element method with high precision on a quantum annealer using only a few qubits. A small-scale problem, involving only 6 qubits for 3 continuous variables, allowed us to assess the performances of AQAE when the optimization part is solved on a D-Wave’s quantum annealer, via a classical simulated annealing algorithm, or exactly. It has been concluded that the method is robust with respect to the non-adiabaticity that can be induced by sub-exponential annealing times and noise in current quantum hardware. Afterwards, a larger problem involving 50 qubits for 25 continuous variables has been solved. It allowed us to highlight the existence of integrated control errors (ICE) that did not appear for the small-scale problem and to establish that the robustness of AQAE with respect to ICE is problem dependent. As ICE are expected to reduce in the next generation of quantum annealers, the range of problems that are robust with respect to ICE is expected to increase. As a perspective, a more detailed finite-size scaling of the performance of the algorithm with respect to different noise sources could be realized, in order to determine e.g., which noise source is the most detrimental.

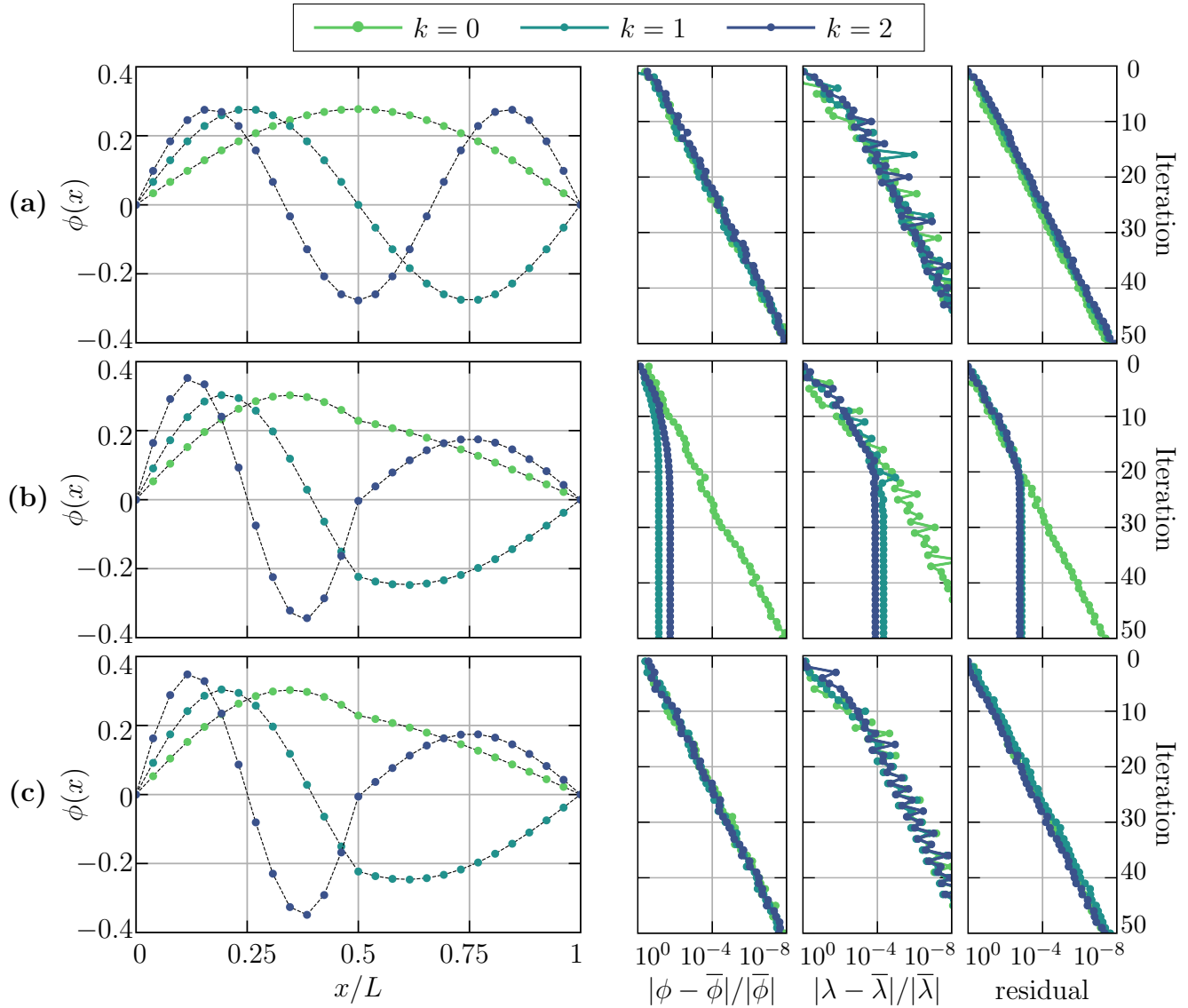


Figure 4: **50-qubit gEVP problem**: solution of the gEVP using the AQAE algorithm ($\phi(x)$ in colored dots) and a classical gEVP solver ($\bar{\phi}(x)$ in dashed lines) **(a)** in a homogeneous material (vacuum) using D-Wave’s quantum annealer, **(b)** in a heterogeneous material (SiO₂-vacuum, $l = L/2$) using D-Wave’s quantum annealer; **(c)** in a heterogeneous material (SiO₂-vacuum, $l = L/2$) using a classical QUBO solver.

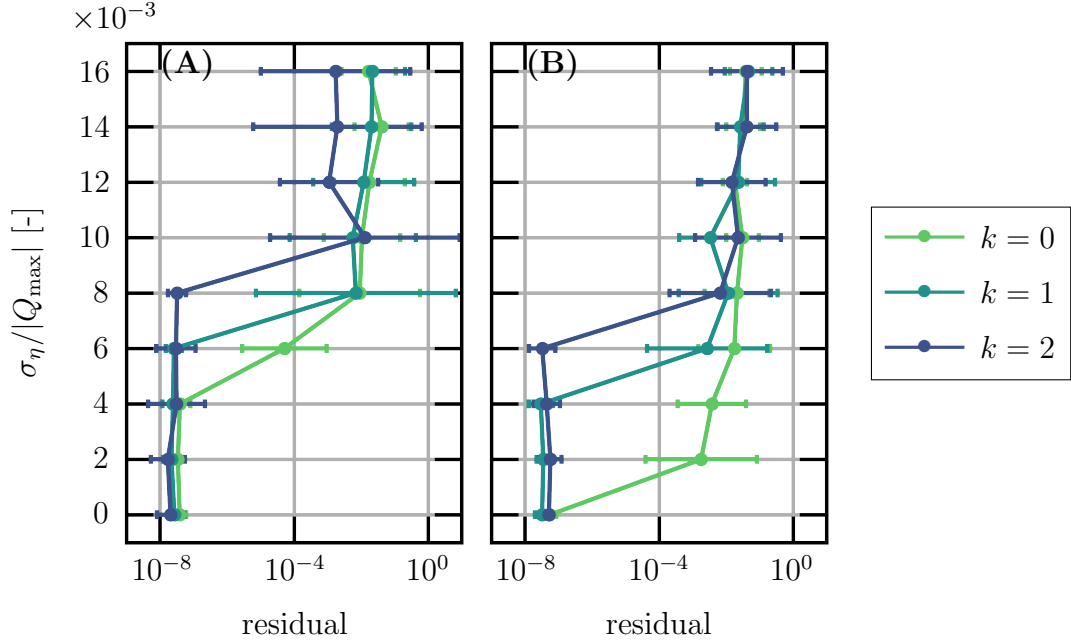


Figure 5: Relative residual as a function of the perturbation σ_η (A) in a homogeneous material (vacuum) (B) in a heterogeneous material (SiO₂-vacuum, $l = L/2$). Error bars correspond to the standard deviation of the measurements.

A Mathematical developments

A.1 Min-max theorem for gEVPs

In this appendix, the min-max theorem will be derived and generalized to generalized eigenvalue problems.

Lemma 1. *Let H be a hermitian operator that belongs to a Hilbert space \mathcal{H} with eigenvalues ordered such that $\lambda_0 \leq \dots \leq \lambda_{N-1}$ and corresponding eigenvectors $\phi_0, \dots, \phi_{N-1}$. Let $\mathcal{S}_k \subseteq \mathcal{H} \setminus \{\mathbf{0}\}$ with $\dim(\mathcal{S}_k) = N - k$, then*

$$\exists \phi \in \mathcal{S}_k \quad \text{s.t.} \quad \frac{\phi^\dagger A \phi}{\phi^\dagger \phi} \leq \lambda_k.$$

Proof. Dimensional reasonings allows to write

$$\begin{aligned} \dim(\mathcal{S}_k) + \dim(\text{span}(\phi_0, \dots, \phi_k)) &= N + 1 > N \\ \Rightarrow \mathcal{S}_k \cap \text{span}(\phi_0, \dots, \phi_k) &\neq \emptyset. \end{aligned}$$

Hence, for any $\phi \in \mathcal{S}_k \cap \text{span}(\phi_0, \dots, \phi_k)$, it is trivial that the lemma is verified. \square

Theorem 1 (Min-Max Theorem). *Let H and M be Hermitian operators that belong to a Hilbert space \mathcal{H} , with M being positive definite. Let us define a Hilbert space $\mathcal{S}_k \subseteq \mathcal{H} \setminus \{\mathbf{0}\}$ with $\dim(\mathcal{S}_k) = N - k$. Then, the generalized eigenvalues $\{\lambda_i\}$ (with λ_i ordered such that $\lambda_0 \leq \dots \leq \lambda_{N-1}$) of the generalized eigenvalue problem*

$$H\phi = \lambda M\phi$$

are given by

$$\lambda_k = \max_{\mathcal{S}_k} \min_{\phi \in \mathcal{S}_k} R_{H,M}(\phi) = \max_{\mathcal{S}_k} \min_{\phi \in \mathcal{S}_k} \frac{\phi^\dagger H \phi}{\phi^\dagger M \phi},$$

where $R_{H,M}$ denotes the Rayleigh quotient for the (H, M) pair, and ϕ^\dagger denotes the conjugate transpose of ϕ .

Proof. Consider the standard EVP

$$H\phi = \lambda\phi,$$

for Hermitian H . Using the above lemma,

$$\min_{\phi \in \mathcal{S}_k} \frac{\phi^\dagger H \phi}{\phi^\dagger \phi} \leq \lambda_k.$$

Taking $\mathcal{S}_k = \text{span}(\phi_k, \dots, \phi_{N-1})$ gives

$$\min_{\phi \in \mathcal{S}_k} \frac{\phi^\dagger H \phi}{\phi^\dagger \phi} \geq \lambda_k,$$

which concludes the proof. This can be generalized for

$$H\phi = \lambda M\phi$$

with Hermitian positive definite M . Taking the Cholesky decomposition $M = L^\dagger L$, the variational functional becomes

$$\frac{\phi^\dagger H \phi}{\phi^\dagger M \phi} = \frac{\phi^\dagger H \phi}{\phi^\dagger L^\dagger L \phi} = \frac{\phi^\dagger L^\dagger L^{-\dagger} H L^{-1} L \phi}{\phi^\dagger L^\dagger L \phi} = \frac{\mathbf{y}^\dagger \tilde{H} \mathbf{y}}{\mathbf{y}^\dagger \mathbf{y}},$$

where $\tilde{H} = L^{-\dagger} H L^{-1}$ and $\mathbf{y} = L\phi$. This shows the equivalence between the variational formulation of standard and generalized EVPs. \square

A.2 Continuous to binary quadratic functions mapping

Once a continuous-to-binary mapping $\phi_j \rightarrow \phi_{j,\min} + \mathbf{b}^T \mathbf{q}_j$ is defined, any quadratic expression $\phi^T A \phi$, $\phi \in \mathbb{R}^N$ can be written as a quadratic binary expression as follows

$$\begin{aligned} \phi^T A \phi &\approx \phi_{\min}^T A \phi_{\min} + [\mathbf{q}_0^T \mathbf{b} \cdots \mathbf{q}_{N-1}^T \mathbf{b}] A \phi_{\min} \\ &+ \phi_{\min}^T A \begin{bmatrix} \mathbf{b}^T \mathbf{q}_0 \\ \vdots \\ \mathbf{b}^T \mathbf{q}_{N-1} \end{bmatrix} + [\mathbf{q}_0^T \mathbf{b} \cdots \mathbf{q}_{N-1}^T \mathbf{b}] A \begin{bmatrix} \mathbf{b}^T \mathbf{q}_0 \\ \vdots \\ \mathbf{b}^T \mathbf{q}_{N-1} \end{bmatrix} \\ &= \phi_{\min}^T A \phi_{\min} + \mathbf{q}^T \begin{bmatrix} D_1 & & 0 \\ & \ddots & \\ 0 & & D_N \end{bmatrix} \mathbf{q} + \mathbf{q}^T \begin{bmatrix} A_{11} \mathbf{b} \mathbf{b}^T & \cdots & A_{1N} \mathbf{b} \mathbf{b}^T \\ \vdots & \ddots & \vdots \\ A_{N1} \mathbf{b} \mathbf{b}^T & \cdots & A_{NN} \mathbf{b} \mathbf{b}^T \end{bmatrix} \mathbf{q}, \end{aligned}$$

where

$$\mathbf{q} = \begin{bmatrix} \mathbf{q}_0 \\ \vdots \\ \mathbf{q}_{N-1} \end{bmatrix}, \quad D_i = \text{diag}(((A_{ii} + A_{:i}) \cdot \phi_{\min}) \mathbf{b}).$$

By defining

$$Q_A = \begin{bmatrix} D_1 & & 0 \\ & \ddots & \\ 0 & & D_N \end{bmatrix} + \begin{bmatrix} A_{11}\mathbf{b}\mathbf{b}^T & \cdots & A_{1N}\mathbf{b}\mathbf{b}^T \\ \vdots & \ddots & \vdots \\ A_{N1}\mathbf{b}\mathbf{b}^T & \cdots & A_{NN}\mathbf{b}\mathbf{b}^T \end{bmatrix},$$

we can write the continuous quadratic function as

$$\boldsymbol{\phi}^T A \boldsymbol{\phi} \approx \boldsymbol{\phi}_{\min}^T A \boldsymbol{\phi}_{\min} + \mathbf{q}^T Q_A \mathbf{q}. \quad (20)$$

The variational function handled by the IQAE is of the form

$$f_k(\boldsymbol{\phi}) = \boldsymbol{\phi}^\dagger H \boldsymbol{\phi} - \gamma \boldsymbol{\phi}^\dagger M \boldsymbol{\phi} + \xi_k(\boldsymbol{\phi}),$$

which, using Eq. (20), becomes

$$\begin{aligned} f_k(\mathbf{q}) &= \boldsymbol{\phi}_{\min}^T H \boldsymbol{\phi}_{\min} + \mathbf{q}^\dagger Q_H \mathbf{q} - \gamma (\boldsymbol{\phi}_{\min}^T M \boldsymbol{\phi}_{\min} + \mathbf{q}^\dagger Q_M \mathbf{q}) + \sum_{m=0}^{k-1} \beta_m (\boldsymbol{\phi}_{\min}^T P_{M, \phi_m} \boldsymbol{\phi}_{\min} + \mathbf{q}^\dagger Q_{P_{M, \phi_m}} \mathbf{q}) \\ &= \mathbf{q}^T Q \mathbf{q} + \text{const.} \end{aligned}$$

in terms of binary variables.

B Solvers parameters

B.1 Solver parameters for the 6 qubits problems

| N | K | N_δ | N_γ | α | numreads | t_a |
|-----|-----|------------|------------|----------|-----------|---------------|
| – | – | – | – | – | – | μs |
| 3 | 2 | 25 | 4 | 1/2 | {1, 4, 8} | {1, 10} |

Table 1: Solver parameters for the 6-qubit problem.

B.2 Solver parameters for the 50-qubit problem

| N | K | N_δ | N_γ | α | numreads | t_a |
|-----|-----|------------|------------|--------------|----------|---------------|
| – | – | – | – | – | – | μs |
| 25 | 2 | 50 | 2 | $\sqrt{2}/2$ | 1000 | 100 |

Table 2: Solver parameters for the 50-qubit problem.

C Complementary results

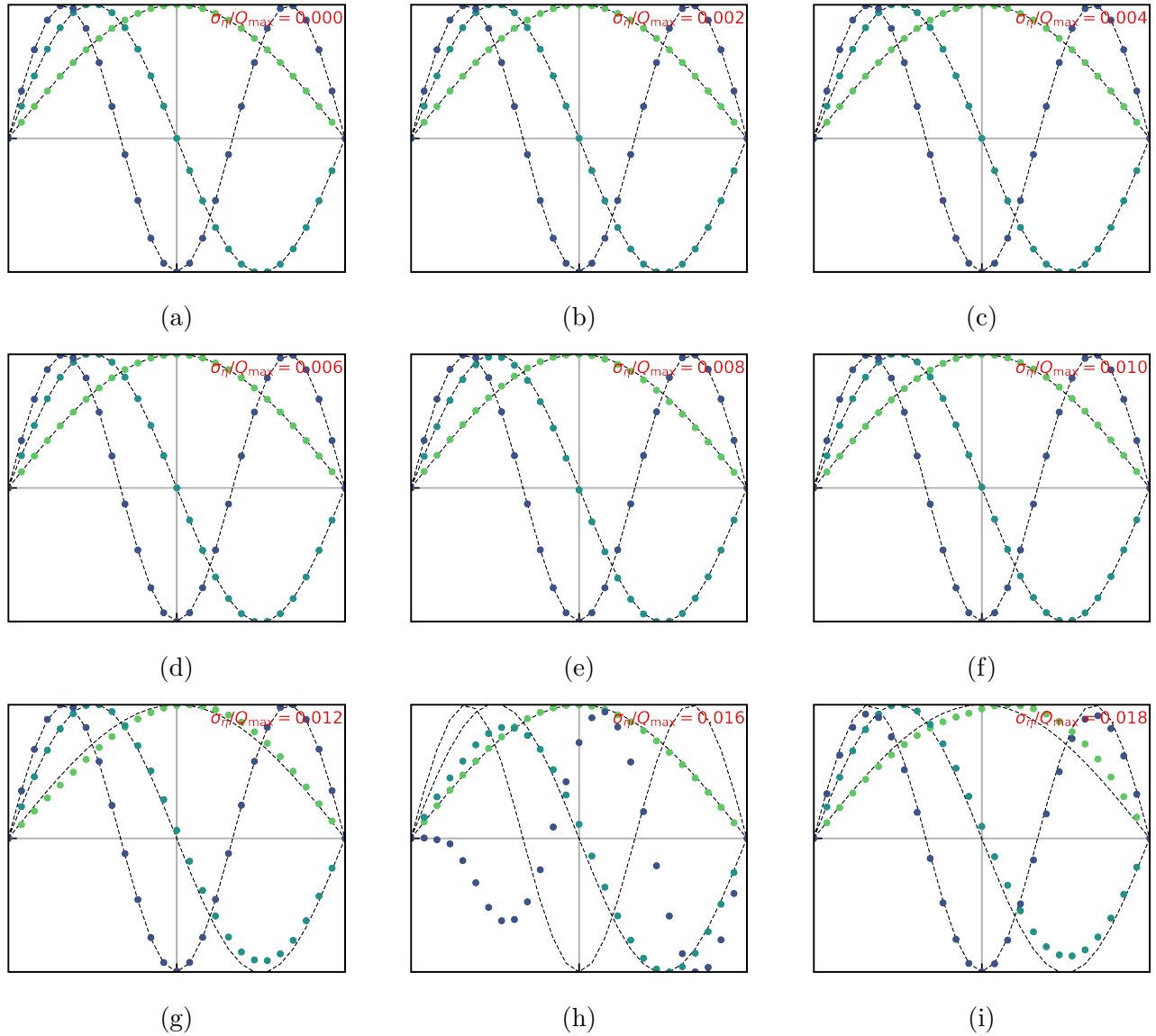


Figure 6: Solution of the gEVP for the 50-qubit problem with homogeneous (vacuum) material. Colored dots are generated using AQAE with a classical qubo solver with additional artificial gaussian ICE of standard deviation σ_η . Dashed lines generated using a classical EVP solver.

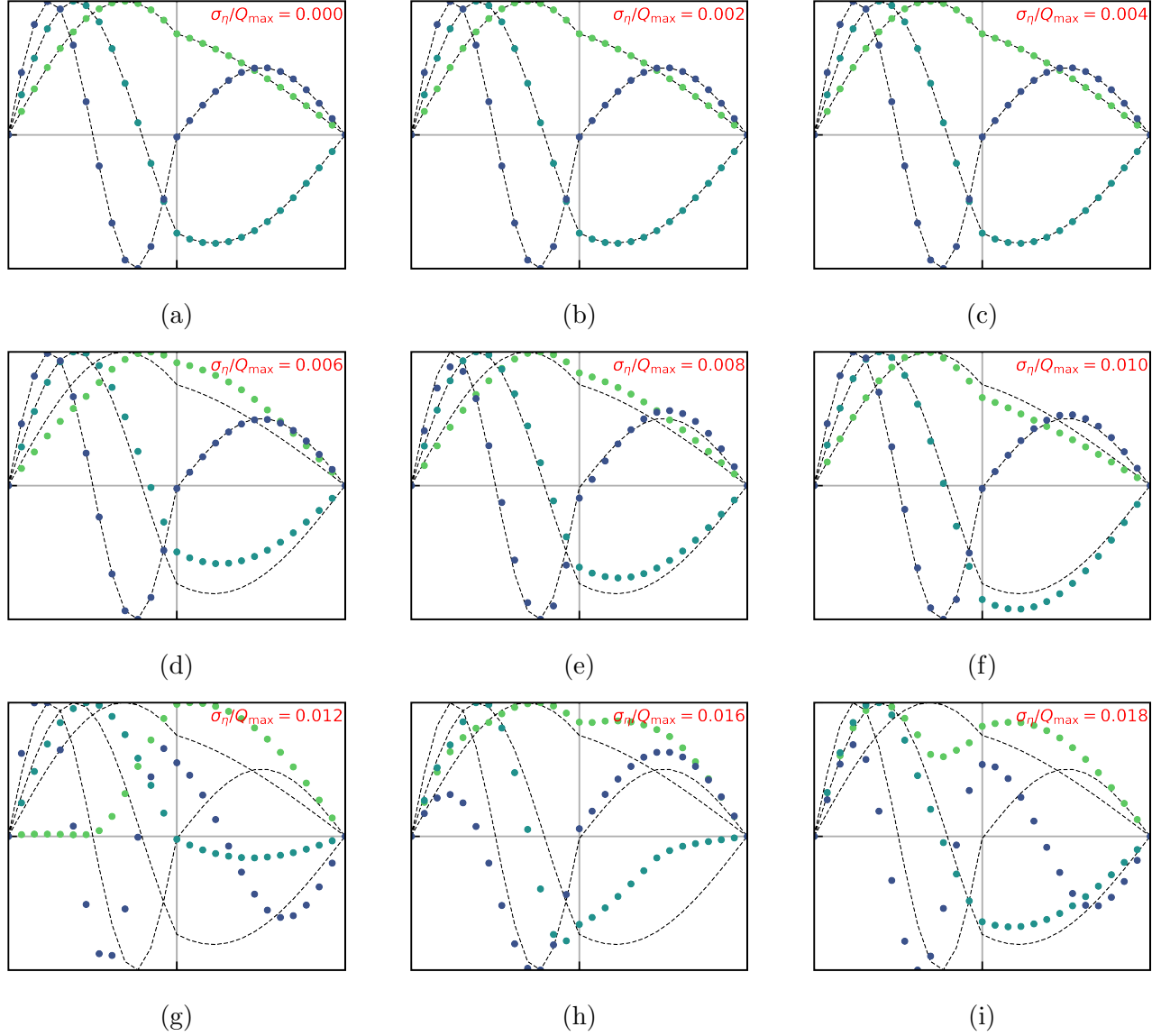


Figure 7: Solution of the gEVP for the 50-qubit problem with heterogeneous (SiO₂-vacuum, $l = L/2$) material. Colored dots are generated using AQAE with a classical qubo solver with additional artificial gaussian ICE of standard deviation σ_η . Dashed lines generated using a classical EVP solver.

References

- [1] S. M. L. Pfaendler, K. Konson, and F. Greinert, “Advancements in quantum computing—viewpoint: Building adoption and competency in industry,” *Datenbank-Spektrum*, vol. 24, pp. 5–20, Mar 2024.
- [2] J. W. Z. Lau, K. H. Lim, H. Shrotriya, and L. C. Kwek, “Nisq computing: where are we and where do we go?,” *AAPPS Bulletin*, vol. 32, p. 27, Sep 2022.
- [3] H. Liu, G. H. Low, D. S. Steiger, T. Häner, M. Reiher, and M. Troyer, “Prospects of quantum computing for molecular sciences,” *Materials Theory*, vol. 6, p. 11, Mar 2022.
- [4] S. Golestan, M. Habibi, S. Mousazadeh Mousavi, J. Guerrero, and J. Vasquez, “Quantum computation in power systems: An overview of recent advances,” *Energy Reports*, vol. 9, pp. 584–596, 2023.
- [5] P. Hauke, H. G. Katzgraber, W. Lechner, H. Nishimori, and W. D. Oliver, “Perspectives of quantum annealing: methods and implementations,” *Reports on Progress in Physics*, vol. 83, p. 054401, may 2020.
- [6] D. Aharonov, W. van Dam, J. Kempe, Z. Landau, S. Lloyd, and O. Regev, “Adiabatic quantum computation is equivalent to standard quantum computation,” in *45th Annual IEEE Symposium on Foundations of Computer Science*, pp. 42–51, 2004.
- [7] A. Lucas, “Ising formulations of many np problems,” *Frontiers in physics*, vol. 2, p. 5, 2014.
- [8] N. Herrmann, D. Arya, M. W. Doherty, A. Mingare, J. C. Pillay, F. Preis, and S. Prestel, “Quantum utility – definition and assessment of a practical quantum advantage,” in *2023 IEEE International Conference on Quantum Software (QSW)*, IEEE, July 2023.
- [9] A. J. Daley, I. Bloch, C. Kokail, S. Flannigan, N. Pearson, M. Troyer, and P. Zoller, “Practical quantum advantage in quantum simulation,” *Nature*, vol. 607, pp. 667–676, Jul 2022.
- [10] P. Arnault, P. Arrighi, S. Herbert, E. Kasnetsi, and T. Li, “A typology of quantum algorithms,” 2024.
- [11] S. A Rahman, R. Lewis, E. Mendicelli, and S. Powell, “Su (2) lattice gauge theory on a quantum annealer,” *Physical Review D*, vol. 104, no. 3, p. 034501, 2021.
- [12] A. Teplukhin, B. K. Kendrick, and D. Babikov, “Calculation of molecular vibrational spectra on a quantum annealer,” *Journal of chemical theory and computation*, vol. 15, no. 8, pp. 4555–4563, 2019.
- [13] M. Illa and M. J. Savage, “Basic elements for simulations of standard-model physics with quantum annealers: Multigrid and clock states,” *Physical Review A*, vol. 106, no. 5, p. 052605, 2022.
- [14] V. Kumar, N. Baskaran, V. Prasanna, K. Sugisaki, D. Mukherjee, K. Dyllal, and B. Das, “Accurate computation of relativistic excitation energies using quantum annealing,” *arXiv preprint arXiv:2212.01801*, 2022.
- [15] J. J. Sakurai and E. D. Commins, “Modern quantum mechanics, revised edition,” 1995.

- [16] B. Apolloni, C. Carvalho, and D. De Falco, “Quantum stochastic optimization,” *Stochastic Processes and their Applications*, vol. 33, no. 2, pp. 233–244, 1989.
- [17] C. McGeoch, *Adiabatic Quantum Computation and Quantum Annealing*. Springer, 2014.
- [18] S. Jansen, M.-B. Ruskai, and R. Seiler, “Bounds for the adiabatic approximation with applications to quantum computation,” *Journal of Mathematical Physics*, vol. 48, no. 10, 2007.
- [19] A. Elgart and G. A. Hagedorn, “A note on the switching adiabatic theorem,” *Journal of Mathematical Physics*, vol. 53, no. 10, 2012.
- [20] J. Biamonte, “Nonperturbative k-body to two-body commuting conversion hamiltonians and embedding problem instances into ising spins,” *Physical Review A*, vol. 77, no. 5, p. 052331, 2008.
- [21] R. Babbush, P. J. Love, and A. Aspuru-Guzik, “Adiabatic quantum simulation of quantum chemistry,” *Scientific reports*, vol. 4, no. 1, p. 6603, 2014.
- [22] A. Teplukhin, B. K. Kendrick, and D. Babikov, “Solving complex eigenvalue problems on a quantum annealer with applications to quantum scattering resonances,” *Physical Chemistry Chemical Physics*, vol. 22, no. 45, pp. 26136–26144, 2020.
- [23] A. Teplukhin, B. K. Kendrick, S. Tretiak, and P. A. Dub, “Electronic structure with direct diagonalization on a d-wave quantum annealer,” *Scientific reports*, vol. 10, no. 1, p. 20753, 2020.
- [24] A. Teplukhin, B. K. Kendrick, S. M. Mniszewski, S. Tretiak, and P. A. Dub, “Sampling electronic structure quadratic unconstrained binary optimization problems (qubos) with ocean and mukai solvers,” *Plos one*, vol. 17, no. 2, p. e0263849, 2022.
- [25] A. Teplukhin, B. K. Kendrick, S. M. Mniszewski, Y. Zhang, A. Kumar, C. F. Negre, P. M. Anisimov, S. Tretiak, and P. A. Dub, “Computing molecular excited states on a d-wave quantum annealer,” *Scientific reports*, vol. 11, no. 1, p. 18796, 2021.
- [26] W.-B. Ewe, D. E. Koh, S. T. Goh, H.-S. Chu, and C. E. Png, “Variational quantum-based simulation of waveguide modes,” *IEEE Transactions on Microwave Theory and Techniques*, vol. 70, no. 5, pp. 2517–2525, 2022.
- [27] D-Wave, “D-wave system documentation.” <https://docs.dwavesys.com/docs/latest/>. Accessed: October 7, 2024.
- [28] S. Srivastava and V. Sundararaghavan, “Box algorithm for the solution of differential equations on a quantum annealer,” *Physical Review A*, vol. 99, no. 5, p. 052355, 2019.
- [29] R. Conley, D. Choi, G. Medwig, E. Mroczko, D. Wan, P. Castillo, and K. Yu, “Quantum optimization algorithm for solving elliptic boundary value problems on d-wave quantum annealing device,” in *Quantum Computing, Communication, and Simulation III*, vol. 12446, pp. 53–63, SPIE, 2023.
- [30] V.-D. Nguyen, L. Wu, F. Remacle, and L. Noels, “A quantum annealing-sequential quadratic programming assisted finite element simulation for non-linear and history-dependent mechanical problems,” *European Journal of Mechanics-A/Solids*, vol. 105, p. 105254, 2024.

- [31] D. Bertsimas and J. Tsitsiklis, “Simulated annealing,” *Statistical science*, vol. 8, no. 1, pp. 10–15, 1993.
- [32] H. Oshiyama, S. Suzuki, and N. Shibata, “Classical simulation and theory of quantum annealing in a thermal environment,” *Phys. Rev. Lett.*, vol. 128, p. 170502, Apr 2022.
- [33] B. Gulácsi and G. Burkard, “Signatures of non-markovianity of a superconducting qubit,” *Phys. Rev. B*, vol. 107, p. 174511, May 2023.